RS(85)N32
MFCIWP(85)P18
CLM-R262

CURLIM
A RATE LIMITED MCFI MODEL FOR SODIUM
Part I: Fundamental Model and Parameter Studies

D. F. Fletcher
Culham Laboratory, Abingdon, Oxfordshire, OX14 3DB, UK

Abstract

This paper describes the first stage in the development of a rate limited MFCI model for sodium. The model assumes one dimensional geometry with an interaction zone surmounted by a sodium slug which compresses a fixed mass of overgas as it moves. The model allows for compressibility effects in the initial response of the slug but changes to an inertial load when these become unimportant. The overall heat transfer from fuel to coolant in the interaction zone is modelled by separate treatments of fuel fragmentation and heat transfer per unit area. Fuel fragmentation is modelled by allowing the melt surface area to increase linearly over a user-specified time; heat transfer per unit area is modelled using specified heat transfer coefficients. It is intended to modify the model to include a mechanistic treatment of heat transfer and fragmentation in a future version of the code.

The model has been applied to examine the effect of the heat transfer, hydrodynamic, and cover gas parameters. The first results obtained from the model have highlighted the importance of modelling a rapid heat transfer stage correctly. In particular they have shown the importance of knowing whether a metal-insulator transition occurs in sodium, and if so for what thermodynamic conditions it occurs.

December 1985

ISBN 085311 145 6

CONTENTS

Nomenclature

A - melt surface area

C_o - speed of sound

C_m - heat capacity of melt

C_f - friction factor

C_v - specific heat at constant volume

d - melt particle diameter

D_H - hydraulic diameter of slug

e - specific internal energy

g - acceleration due to gravity

h - heat transfer coefficient

L - slug length

m - mass

P - pressure

q - heat added to unit mass of sodium

S - interfacial area between slug and MFCI zone

T - temperature

t - time

V - volume

v - velocity

W - work done on overgas

x - quality

z - distance

Greek symbols

ν - specific volume

ρ - density

τ_{ac} - acoustic transmission time

τ_{f} - fragmentation time

γ - isentropic exponent for overgas

γ_{v} - thermal pressure coefficient

Γ_{ν} - Gruneisen coefficient

Suffixes

∞ - final value

o - initial value

crit - critical value

cg - cover gas

f - final value (for overgas)

i - initial value (for overgas)

ℓ - liquid

m - melt

s - sodium

sat - saturation line value

v - vapour

1. Introduction

It has long been recognised that explosive rates of vapour generation could arise in hypothetical severe accidents in sodium-cooled fast reactors if molten fuel mixes with liquid coolant. This phenomenon has become known as a molten fuel coolant interaction (MFCI) [1].

Thermodynamic models of such events enable an upper bound on the conversion of thermal to mechanical energy to be calculated [2]. However, this upper bound is very conservative, predicting efficiencies which are at least an order of magnitude greater than those observed in experiments with real materials [3]. Also, whilst thermodynamic models avoid the need to understand the complicated physics involved in the interaction process, they cannot be used to determine pressure-time histories or to determine reactivity increases caused by the expulsion of liquid sodium from within a single sub-assembly or the reactor core.

These requirements have led to the development of numerous models which seek to model the rate-limited processes which occur during an MFCI. These models use simplified physics in a zero or one-dimensional geometry to predict transient sodium temperatures and pressures, and the kinetic energy of any liquid sodium which is expelled from the vicinity of the MFCI. A brief review of some of these models will be given in section 2.

A rate-limited MFCI model has been developed by the author with the aim of combining the best features from the variety of models currently available. The model assumes one dimensional geometry with an interaction zone surmounted by a sodium slug. In addition some new physics, such as the effect of adding an overgas above the slug has been included. In this paper the basic model equations are described, together with the results obtained from some studies of the effect of various parameters. The aim has been to produce a flexible computer code, named CURLIM (Culham Rate Limited MFCI Model), which can be used to examine the effect of uncertain physics or the role played by a specified parameter. Ultimately it is hoped to develop the model into a predictive tool for use in the study of

some aspects of severe accidents (especially those occurring within a single sub-assembly) or for use in the analysis of experiments carried out to simulate them.

2. Previous Work

Numerous rate-limited models have been constructed in the past for use in assessing the consequences of sub-assembly accidents [4,5] and whole core accidents [6]. An extensive review and comparison of these models was carried out by Jakeman [7]. This review included both a detailed comparison of the modelling, and a comparison of the predicted peak pressures and sodium explusion times for a specified test case. The models produced a wide range of different solutions reflecting the different treatments of physical processes in them, but the exercise did not suggest that any model had any special merit over any other.

In all the models molten fuel is assumed to come into contact with sodium in an interaction zone which is surmounted by a slug of sodium. Energy is transferred to the sodium in the interaction zone causing its pressure to rise, which in turn causes expansion of the mixing zone. The rate of expansion is limited by the presence of the sodium slug, which is assumed to be either compressible (acoustic phase) or incompressible (inertial phase) during different phases of the calculation. Other physics, such as the effect of any fission gas present, the effect of friction and pressure loss at sub-assembly exits, and the loss of heat to cold clad was also examined.

Most of the models are based on the work of Cho and Wright [4,6,8] from Argonne. These authors carried out extensive parametric surveys to examine the effect of various assumptions about the behaviour of the slug, the heat transfer mechanisms, and fuel size and fragmentation rates. This work was extended by Fishlock [5] who produced a model (EXPEL) of MFCI's in fast reactor sub-assemblies. Caldarola [9,10] has developed a similar parametric model and added very detailed models for heat transfer for both the case when the sodium is a single phase liquid, and for the situation

which develops as vapour is formed and the heat transfer resistance between the fuel and coolant increases.

In the next section the present model will be described and the important modelling features will be compared with those used in the models outlined above.

3. Model Description

In this section the rate limited model is developed and the simplifying assumptions made are stated and justified. Figure 3.1 shows the assumed geometry. The following assumptions are made:-

(i) The geometry is 1D with a slug of sodium surmounting an interaction zone. The interface between the MFCI zone and the sodium slug is of arbitrary shape, with fixed surface area S and hydraulic diameter D_H.

(ii) There is no heat loss from the MFCI zone to its surroundings. This is a simplifying assumption which will be modified in a future version of the model to allow for heat loss by condensation of heated sodium onto the slug and possibly to allow for heat conduction from the MFCI zone to surrounding structures.

(iii) A spatially constant temperature and pressure are assumed to exist within the interaction zone. These assumptions are conventional in parametric models [5,8,9], since they allow the formulation of a model in terms of a set of ordinary differential equations. Because of the highly transient nature of MFCI processes, spatial, as well as temporal, gradients of pressure and temperature will exist. However, the details of the heat transfer and fragmentation processes which determine these gradients are, as yet, unknown.

(iv) The melt is assumed to be uranium dioxide at a user specified initial temperature. The melt density is assumed to be 8700 kg/m^3 initially, and to remain constant as the melt cools. Thus the expansion of the sodium allowed by the contraction of the melt as it cools is not

allowed for, causing peak pressures to be over-estimated. The melt specific heat capacity was replaced by a constant linear regression coefficient (503 J/kg K) fitted to the enthalpy-temperature plot in order to allow for the latent heat released upon melt freezing.

In the next three sections the heat transfer and fragmentation model, the hydrodynamic treatment, and the EOS data used will be described.

3.1 Heat Transfer and Fragmentation Model

The specification of a heat transfer model includes both a model for the heat transfer processes taking place and a model of the increase in interfacial area due to fragmentation. Many workers have combined these processes into a single model.

The most common model of fragmentation is to assume a constant surface area caused by instantaneous fragmentation at the start of the interaction. Other models have allowed for a time dependent surface area resulting from a finite fragmentation rate.

It has become conventional to split the heat transfer model into two phases, depending on whether vapour has been formed or not.

3.1.1 Phase A - Single phase coolant

During this stage the melt is in contact with liquid (or high-density supercritical) sodium and the dominant resistance to heat transfer is the thermal conductivity of the melt. Many of the previous parametric models have used one of the three alternative models suggested by Cho et al. [6,8]. These are:-

(i) a quasi-steady-state model where a constant heat transfer coefficient equal to the melt thermal conductivity divided by the particle radius is used. It is claimed [9] that this represents "a finite rate of fragmentation and mixing" and that this approximation implies that "by the time the fragmentation of the fuel is completed there already exists a

significant temperature gradient in the fuel particles" but there seems to be little justification for its use.

(ii) a transient conduction model where a linear temperature profile in the melt is assumed over a calculated penetration thickness. This model represents instantaneous fragmentation and mixing, with heat transfer limited only by the thermal conductivity of the melt.

(iii) a finite fragmentation and mixing rate model where a user specified time constant can be used to examine the effect of fragmentation rate. The asymptotic heat transfer rate is the same as that produced by the quasi-steady-state model.

Caldarola [9,10] follows (ii) above but solves the heat conduction equation rigorously. Other models use more approximate solutions [7].

3.1.2 Phase B - Two phase coolant

Complete heat transfer cut-off whenever any vapour is present is the simplest assumption which can be made and leads to the smallest estimate of work done. In reality this approach is too simple, since radiation and conduction heat transfer will still occur. Caldarola [9,10] assumes that a particle of melt remains suspended inside a vapour bubble with the weight of the particle being balanced by the upward drag of the vapour. The liquid is heated by conduction through the vapour layer and direct radiation. Other models assume that the contact area between melt and liquid is proportional to the liquid volume fraction. A detailed review of other ad hoc models is given in reference 7.

3.1.3 Present Model

In the present model it was decided to start with the simplest possible heat transfer and fragmentation models for the initial stage of model development. Thus it was decided to assume two different constant heat transfer coefficients during phases A and B. The melt temperature is determined by using a lumped energy balance. Although this is clearly

incorrect for high heat transfer coefficients (> 10^3 W/m^{2}K) [11] it provides a useful step in the development of a more complex model. Making use of these assumptions gives

$$\frac{dT_m}{dt} = - h A_m (T_m - T_s)/m_\infty C_m \qquad (3.1)$$

A subroutine is provided in the code to evaluate the melt surface area as a function of time. At present the details of the fragmentation process are unknown [1,8], and as a first step in model development the melt surface area was simply assumed to increase linearly with time, so that

$$A_m = A_\infty \, t/\tau_f \qquad 0 < t < \tau_f$$

$$= A_\infty \qquad t > \tau_f \qquad (3.2)$$

where:

$$A_\infty = \frac{6m_m}{\rho_m d_m} \qquad (3.3)$$

3.2 Hydrodynamic Models

It is usual to use an approximate treatment, rather than solve the full compressible flow momentum equation, to determine the motion of the sodium slug. There are two approaches which have been used.

The first is to treat the slug as incompressible and to use Newton's second law to determine its motion. This approach over-estimates the interaction pressures during the initial phase because it does not allow for the compressibility of the sodium [8]. This is termed an inertial load.

The second approach allows for the compressibility of the sodium by modelling the propagation of a shock wave into the sodium. The shock wave is treated as a sound wave so that it propagates into the slug with a

velocity equal to the local sound speed. This approximation is reasonable for a large range of shock pressures, (c.f. very good approximation up to 67 MPa for water [12]). This model produces more realistic pressures for the initial stage of the MFCI, since some relief of pressure is allowed as soon as pressure is generated in the MFCI zone. This is termed an acoustic constraint.

It is generally agreed that a satisfactory procedure is to use an acoustic constraint initially and then to change to an inertial constraint when the pressure in the interaction zone has fallen sufficiently for compressibility effects to be negligible. The acoustic wave propagates into the sodium slug and is reflected at the top of the column to form a rarefaction wave which relieves pressure as it returns. On the return of the rarefaction wave to the MFCI zone the rarefaction wave will, in general, be partially transmitted and partially reflected (see [5,13]). If vapour has formed in the interaction zone the rarefaction wave will be largely reflected, and it is a good approximation to change to an inertial load. If no vapour is present an appreciable fraction of the wave will be transmitted leading to rapid depressurization of the interaction zone, and consequent vapour production. This may be modelled to an adequate approximation by assuming complete transmission of the rarefaction wave and continuing with the acoustic model until vapour forms.

The treatment of the compressible stage of slug motion is in reality much more complicated than the simple picture described above. Because the pressure in the interaction zone is not constant, different parts of the slug will be moving with different particle velocities. Thus the returning rarefaction wave will not bring the particles just to rest, but will cause cavitation in the slug. However, effects such as this are beyond the scope of the present model and will be ignored.

The approach described above was used by Fishlock in the EXPEL code [5]. Caldorola [9] changed to an inertial load as soon as the rarefaction wave returned to the interaction zone, whether vapour was present or not. Cho et al. [8] examined the effect of each type of constraint but did not combine them.

3.2.1 Present Model

In the present model it was decided to use the same approach as that used by Fishlock. A derivation of the relevant equations can be found in references 9 and 13, and they will simply be stated here.

In the acoustic stage the motion of the interface is determined from

$$\frac{dz}{dt} = \frac{1}{\rho_o C_o} \left(P(t) - P_o + 2 \sum_{k=0}^{n-1} (P_k - P_o) \right) \qquad (3.4)$$

where P_o is the initial pressure in the interaction zone and is given by

$$P_o = P_i + \rho_o g L \qquad (3.5)$$

P_k is the pressure in the interaction zone at time $t - (n-k)\tau_{ac}$ and

$$n = \text{int} \left[t/\tau_{ac} \right] \qquad (\text{int} \equiv \text{integer part of}) \qquad (3.6)$$

τ_{ac} is the time taken for the sound wave to propagate to the top of the slug and return and is given by

$$\tau_{ac} = 2L/C_o \qquad (3.7)$$

This solution is applied until $t = \tau_{ac}$ if vapour is present at time τ_{ac}, or until vapour is formed if no vapour is present at time $t = \tau_{ac}$. When the mass ratio of melt to sodium is very high it is necessary to change to an inertial model before the thermodynamic trajectory of the sodium entered the two phase region, since the sodium specific volume is increased significantly without the formation of vapour. In this case the calculation switches to an inertial model at $v=v_{crit}$ if $t>\tau_{ac}$ or at $t=\tau_{ac}$ if $v \geq v_{crit}$.

During the inertial stage the motion of the interface between the heated and unheated coolant is determined using Newton's second law to give

$$\frac{d^2z}{dt^2} = \frac{P - P_{cg}}{\rho_o L} - g - \frac{2C_f}{D_H}\left(\frac{dz}{dt}\right)^2 \qquad (3.8)$$

where C_f is the appropriate friction factor.

At the change-over time two initial conditions on z are required. The value of z at the change-over time is known from the acoustic calculation. The second initial condition is determined from conservation of momentum which gives

$$\left.\frac{dz}{dt}\right|_{t=t_c} = \frac{1}{\rho_o L}\int_o^{t_c}(P-P_o)\,dt \qquad (3.9)$$

Thus equations (3.4) and (3.8) together with condition (3.9) allow the motion of the interface to be calculated.

3.2.2 Pressure Boundary Condition at the top of the Slug

In all previous models (known to the author) the external pressure is assumed to be constant. Cho, Chen and Wright [6] noted that this assumption was incorrect in their Whole Core Accident model but kept the assumption for simplicity. In the present model it was decided to surmount the slug by a closed region containing a fixed mass of gas, which is assumed to be compressed isentropically by the slug. This situation occurs in many MFCI experiments [3] and provides a useful way of measuring the work done by the MFCI, since all the kinetic energy in the slug is converted to potential energy in the gas at the instant the slug comes to rest [14].

Thus the external pressure can be calculated when the position of the slug is known by using

$$PV^{\gamma} = P_o V_o^{\gamma} \qquad (3.10)$$

During the acoustic stage the boundary at the top of the sodium slug is assumed to be perfectly reflecting since the acoustic impedance of the slug is much greater than that of the gas. Compression of the overgas during the acoustic phase was ignored since an a posteriori analysis showed this to be negligible in all cases. When the model switches to an inertial load the cover gas volume and pressure are calculated by making the assumption that the slug length is equal to its initial value and using the position of the MFCI/slug interface at the change-over time.

3.3 Equation of State for Sodium

The modelling of MFCI's requires knowledge of sodium properties for temperatures and pressures well outside the range of the available experimental data. In addition the thermodynamic path of the sodium in the P-V plane crosses zone boundaries during the interaction, so that different forms of the EOS are needed in different stages of the calculation. Figure 3.2 shows the general form of the P-V plane and illustrates the four different regions of interest in the modelling of MFCI's. These are:

(i) Subcooled liquid region

(ii) Superheated gas region

(iii) Two-phase region

(iv) Supercritical region

The treatment used in each of these regions will now be described.

3.3.1 Subcooled Liquid and Superheated Gas

The subcooled liquid region and the superheated gas region can be treated in the same way. There are essentially three different approaches which have been used.

Cho, Irvin and Wright [8] determined the pressure from the volume and temperature by using the thermal expansion coefficient, α_p, and the isothermal compressibility, β_T. They assumed that these were a function of temperature only and thus were able to use the available saturation curve values. This approach was also used by Caldarola. However, α_p and β_T have been shown to depend on both pressure and temperature [7, 15, 17] so that this approach is not acceptable.

Fishlock [5] assumed that the Gruneisen constant, given by

$$\Gamma_v = v\left(\frac{\partial p}{\partial e}\right)_v \tag{3.11}$$

was a function of volume only.

With this assumption the pressure can be determined from the internal energy and specific volume via

$$P = P_{sat}(v) + \frac{\Gamma_v(v)}{v}\left[\, e(v) - e_{sat}(v) \,\right] \tag{3.12}$$

Recent analysis by Browning [15] shows that this assumption requires the specific heat at constant volume to be independent of temperature. For temperatures above 2300K this is not the case.

Browning [15] and Fink and Leibowitz [17] assume that the thermal pressure coefficient, γ_v, given by

$$\gamma_v = \left(\frac{\partial p}{\partial T}\right)_v \tag{3.13}$$

is a function of volume only. There is however no direct experimental confirmation of this for sodium. Using this assumption the pressure can be determined from the specific volume and temperature using

$$P(\nu,T) = P_{sat}(\nu) + \gamma_v(\nu) \left[T - T_{sat}(\nu)\right] \qquad (3.14)$$

This is the approach adopted in the present model with the required data being taken from references 15 and 16. [Note that the EOS produced by Alderson [16] uses critical constants which are considerably in error (P_{crit} = 41.36 MPa instead of 25.98 MPa). Browning [15] has corrected this to take into account the latest experimental data, so that references 15 and 16 combined allow the necessary properties to be determined over the entire range needed.]

If γ_v is a function of volume only it can easily be shown that the specific heat at constant volume, C_v, is a function of temperature only [16]. Thus for consistency the value of C_v at an arbitrary temperature and pressure should be taken to be equal to the value on the saturation line with the correct temperature. However, C_v becomes unbounded as the temperature approaches the critical point along the saturation curve. This behaviour should only occur near the critical point itself and not at all other points along the critical isotherm. The saturation line data given in reference 16 shows that C_v is reasonably constant except near the critical point. Thus it was decided to use a constant value of the specific heat in each of the compressed liquid and expanded gas regions.

3.3.2 Two Phase Region

In this region the sodium pressure and temperature can be determined from its specific volume and internal energy (or enthalpy) using the lever rule. If the calculated specific volume is ν and the internal energy is e then

$$\nu = x\nu_v + (1-x)\,\nu_l$$

$$e = xe_v + (1-x)\,e_l \qquad (3.15)$$

where x is the quality and v_v, v_l, e_v, and e_l are saturation line values at an unknown pressure. Eliminating x gives

$$\frac{v - v_l}{v_v - v_l} = \frac{e - e_l}{e_v - e_l} \qquad (3.16)$$

which can be used to determine P, and hence T.

The change over from a compressed liquid or expanded gas to a two phase EOS is detected by checking whether the calculated single phase pressure is above or below the saturation pressure. If it is below the calculation switches to a two phase EOS. During the two phase calculations the value of the quality is tested to ensure that it is less than one, if it is not the program switches to a single phase EOS for superheated vapour.

3.3.3 Supercritical Region

In this region there is an almost total absence of experimental data. Most models simply extrapolate the saturation curve into the supercritical region and then continue to use the methods described in the previous sections. The pressure can be determined using the pressure coefficient as described in section 3.3.1 However, there is no reference line from which the internal energy (and hence the specific heat capacity) can be derived. Browning [15] suggests that for supercritical temperatures the internal energy on the critical isochore is directly proportional to the temperature difference $(T_{sup} - T_{crit})$. The constant of proportionality is based on averaging the internal energies on the critical isochore for some small (arbitrary) temperature range directly below T_{crit}, giving

$$e(T,V_{crit}) = e(T_{crit}, V_{crit}) + \bar{C}_v(V_{crit})(T - T_{crit}) \qquad (3.17)$$

The assumption made about the pressure coefficient implies that C_v is a function of temperature alone and from equation (3.17) we have

$$C_v = \left(\frac{\partial e}{\partial T}\right)_v = \bar{C}_v\,(V_{crit}) = \text{constant} \qquad (3.18)$$

Unfortunately it was not possible to determine a value for $\bar{C}_v(V_{crit})$ from Brownings's data, since the data given is not consistent with equation (3.17). Thus a constant value midway between the vapour and liquid values is used as an interim measure.

3.4 Conservation of Energy

In order to use the EOS described in the previous sections it is necessary to be able to determine the temperature (or internal energy) of the sodium when the heat supplied to the sodium and the expansion of the sodium volume have been determined. This is achieved by use of the First Law of thermodynamics applied to the sodium, which gives

$$\frac{dq}{dt} = \frac{de}{dt} + P\,\frac{dv}{dt} \qquad (3.19)$$

and is valid for any quasi-static process of a hydrostatic system [18]. Thus assuming that the sodium is always in thermal equilibrium and only undergoes an infinitesimal change during each timestep, the internal energy of the sodium can be determined using the heat transfer model and hydrodynamic constraint.

Equation (3.19) is in a convenient form for use in the two phase region but requires modification for use in the other regions. Now,

$$de = c_v\,dT + (T\gamma_v - P)\,dv \qquad (3.20)$$

so that equation (3.19) can be written as

$$\frac{dq}{dt} = c_v\,\frac{dT_s}{dt} + T\gamma_v\,\frac{dv}{dt} \qquad (3.21)$$

which relates the change in sodium temperature to the heat added and the change in specific volume. The change in specific volume is related to the velocity of the interface between the MFCI and the slug using

$$\frac{dv}{dt} = \frac{S}{m_s}\left(\frac{dz}{dt}\right) \qquad (3.22)$$

3.5 Solution Procedure

The equations described in the previous four sections were solved using a computer program named CURLIM. The logic of the program is shown in figure 3.3. The relevant ordinary differential equations for each phase of the calculation were integrated using a Runge-Kutta integration routine from the NAG subroutine library [19].

Each calculation was continued until the sodium slug was brought to rest due to compression of the cover gas. The efficiency of conversion of thermal to mechanical energy was calculated by evaluating the work done from

$$W = \frac{1}{(\gamma-1)}\left(P_f V_f - P_i V_i\right) \qquad (3.23)$$

and then defining the efficiency to be

$$\eta = \frac{W}{m_m c_m (T_{mo} - T_{so})} \qquad (3.24)$$

The above quantity gives a useful measure for comparison with experiments and can be used as a test statistic in order to examine the effect of various parameters.

4. Model Results

At present the model is not fully developed since, for instance, it does not contain a mechanistic model of heat transfer. However, it is useful in model development to examine the effect of various parameters to

determine what parts of the model need further improvement. It is also possible to use the model to examine the effect of experimental parameters, such as slug mass and cover gas volume, on the MFCI characteristics and the predicted work yield.

It was decided to choose a base case and then to examine the effect of parameters by varying one parameter at a time. The conditions used for the base case are given in Appendix I and a table showing how these conditions were varied in all the code runs is given in Appendix II. In the next sections the effect of varying various parameters will be examined.

4.1 The Base Case Calculation

The chosen parameters and initial conditions for the base case calculation do not correspond to any particular geometry or postulated accident. They were chosen as representative values appropriate to the analysis of sub-assembly experiments planned in the Molten Fuel Test Facility at Winfrith. The sodium is assumed to be saturated at atmospheric pressure and the melt properties correspond to those of a thermite generated uranium dioxide/molybdenum melt. The heat transfer coefficient used ($h=10^7$ W/m^{2}K) is an effective upper bound, since heat transfer becomes diffusivity-limited in UO_2 for $h>10^7$ W/m^{2}K [11] and the present analysis does not allow for the development of a temperature gradient in the melt. A fragmentation timescale of 1ms was used and the final melt particle size was assumed to be 250 μm. These values are not based on any particular fragmentation process, since no detailed information is available. It has not been possible to compare calculations from the present model directly with other models because insufficient data is reported, particularly concerning the assumed melt surface area and heat transfer rate.

Figure 4.1 shows the variation of pressure in the interaction zone with time for the base case calculation. The peak pressure is about 95MPa with a pressure spike width of about 0.5ms. The calculation continues for 20ms before the sodium slug is brought to rest by compression of the cover gas. At this endstate the pressure in the interaction zone is 0.8 MPa and the pressure in the cover gas is 88 MPa. The final melt temperature is 2390K and the final sodium temperature in the interaction zone is 1454K. The calculated efficiency is 9%.

The calculated efficiency is low because of energy loss due to friction and the large amount of energy which is not transferred from the melt to the sodium. The effect of friction is examined in section 4.4, where it is shown that for this particular calculation friction reduced the efficiency from 15% to 9%. The poor thermal contact between the melt and coolant is also a contributory factor to the low efficiency. In a Hicks-Menzies calculation the melt and coolant are assumed to be in perfect thermal contact, whereas in the present calculation the final melt temperature is approximately 1000K greater than the sodium temperature. Calculating an efficiency based upon energy transferred, rather than energy available for transfer from the melt to the sodium, gives a figure of 18%. For the case where friction is absent this is increased to 32%. Thus in the present study the low efficiency is due to dissipation by friction and thermal disequilibrium between the melt and coolant.

Figures 4.2 and 4.3 show the thermodynamic trajectories of the sodium in the P-T and P-V planes respectively. Figure 4.2 shows that the pressure and temperature initially rise very rapidly and then the pressure falls as the interface between the sodium in the interaction zone and the slug moves upwards rapidly. Eventually the pressure falls sufficiently for vapour to form and the trajectory continues along the saturation line. In the P-V plane the pressure rises very rapidly and then falls as the sodium expands. The rapid fall in pressure with increasing sodium volume is halted as vapour is formed and the sodium expands as a two phase mixture. At the end-state of the calculation approximately half of the sodium mass is in vapour form.

4.2 The Effect of Melt/Coolant Mass Ratio

The melt/coolant mass ratio is one of the most important parameters which has to be input into the model, as this parameter cannot be measured experimentally. The base case calculation uses a melt/sodium mass ratio of 5.

The results are very similar for low mass ratios; however, for higher mass ratios the behaviour is somewhat different. Figure 4.4 shows the sodium trajectory in the P-V plane for a mass ratio of 12. In this calculation the sodium temperature rapidly becomes supercritical and a significant fraction of the thermodynamic path is in the supercritical region. There is a sudden reduction in the rate of pressure fall when the sodium specific volume exceeds the critical volume, even though the calculation does not switch to an inertial model (N.B. although $v > v_{crit}$, $t < \tau_{ac}$). This is because the saturation envelope is very flat on the vapour side of the critical point. Thus when using the pressure coefficient to calculate the pressure from v and T, the calculated pressure falls very slowly because the saturation line properties vary very slowly with volume. The pressure only falls significantly when the calculation switches to an inertial load on return of the rarefaction wave. This peculiar behaviour is due to the method of calculating the pressure and may be an artifact of this particular EOS, rather than a true effect. It will only be possible to investigate this when an improved EOS becomes available.

The efficiency falls as the melt mass is reduced (7.46% for $m_m/m_s=2$) because the sodium is heated to a lower temperature. It also falls for high melt mass fractions (6.87% for $m_m/m_s=12$) because although the sodium is heated to a higher temperature there is much less of it to expand against the same hydrodynamic constraint.

4.3 The effect of Heat Transfer Parameters

The heat transfer parameters form a very important component of the model which is unfortunately not well understood. The effect of changing the heat transfer coefficient in the single phase region was examined. Table 4.1 below shows the effect of this parameter on the efficiency, the peak pressure, and the sodium temperature at the time of vapour formation.

$h(W/m^2K)$	$\eta(\%)$	$P_{max}(MPa)$	$T_s(K)$
10^7	8.96	96	2479
10^6	8.17	41	2458
10^5	3.67	9.2	1880

Table 4.1 - The effect of varying the single phase heat transfer coefficient.

The above table shows that the heat transfer coefficient is a very important parameter in determining the peak pressure. However, although the peak pressure is more than halved by reducing the heat transfer coefficient from $10^7 W/m^2K$ to $10^6 W/m^2K$ the efficiency is not very different. This may be correlated with the sodium temperatures being very similar when vapour forms (which effectively terminates heat transfer). In a calculation with a low heat transfer coefficient there is a reduced peak pressure and the expansion is less rapid, since the interface velocity is lower, allowing the single phase heat transfer rate to be applied for longer. In the case of a heat transfer coefficient of $10^5 W/m^2K$ there is a significant reduction in the efficiency because even with the extended time available for rapid heat transfer (due to the peak pressure being reduced significantly) the total amount of energy transferred is low.

The present heat transfer model needs to be improved to allow for the reduction in heat transfer rate which occurs as a temperature gradient develops in the melt. Previous work by the author [11] has shown this effect to be very important even on the sub-millisecond timescale. The choice of heat transfer models in the two phase region seems to be less important. In the base case calculation a heat transfer coefficient of $10^3 W/m^2K$ was used. This figure represents the appropriate value for

radiation from melt at its initial temperature and so gives an upper bound for radiation heat transfer. Reducing the two phase heat transfer coefficient to zero resulted in a reduction in the efficiency from 8.96% to 8.65% and changed the pressure-time plot imperceptibly.

Changing the fragmentation timescale from 0-10ms changed the predicted efficiencies by very little but changed the MFCI characteristics significantly. Table 4.2 below shows the efficiency, peak pressure, time until vapour production and sodium temperature at that time as a function of fragmentation time.

τ_f(ms)	η(%)	P_{max}(MPa)	Time until vapour formation (ms)	T_s(K)
0	8.35	448	0.43	2453
1	8.96	96	0.72	2479
5	8.61	52	0.86	2469
10	8.17	43	0.90	2461

Table 4.2: The effect of fragmentation time.

The results in the table show that the instantaneous fragmentation (into 250μm particles) calculation predicts a very high peak pressure which causes very rapid expansion of the mixing zone. Conversely, increasing the fragmentation time lowers the peak pressures, prolongs the rapid heat transfer phase and somewhat surprisingly can give higher

efficiencies. The efficiency shows peculiar behaviour, there is a local maximum at a fragmentation time of 1ms, because of the particular choice of parameters for these calculations. Calculations carried out with a heat transfer coefficient of 10^5 W/m^2K gave efficiencies of 4.7% and 3.7% for fragmentation times of 0 and 1 ms, respectively. Thus the anomalous behaviour only occurs when the heat transfer rate is extremely high, either because the heat transfer coefficient is high or the melt surface area is large, and results because the high pressures generated lead to rapid expansion of the interaction zone and early vapour production. In reality the situation would be even more complicated since, for example, the higher pressure shock waves generated when heat transfer is more rapid would dissipate more energy.

In the instantaneous fragmentation case the pressure rise is extremely rapid and approaches constant volume mixing, which is the starting condition for a Hicks-Menzies calculation. In the Hicks-Menzies calculation the sodium almost invariably expands through the supercritical region of the P-V plane. However, in the calculation performed with the present model the initial high pressure is rapidly relieved and the expansion occurs almost entirely in the subcooled liquid and two-phase regions, as shown in figure 4.5.

In the present model the heat flux from the melt to the sodium is proportional to the product of the melt surface area and a constant heat transfer coefficient. Thus increasing the surface area with time is equivalent to having a heat transfer coefficient which increases with time. An improved heat transfer model would give a heat transfer coefficient per unit area which falls with time as temperature gradients are set up in the melt and coolant, so it would be necessary to make the heat transfer coefficient a function of time since the fuel particle was fragmented rather than time since the start of the interaction.

An additional feature which may be important in the modelling of heat transfer is the metal-insulator transition [20]. Theoretical calculations suggest that the thermal conductivity of liquid sodium may fall by several orders of magnitude once it expands beyond a critical volume. This

transition is believed to occur somewhere between a specific volume of $2 \times 10^{-3} m^3/kg$ and the thermodynamic critical volume of $4.68 \times 10^{-3} m^3/kg$ [21, 23]. It has not, as yet, been observed experimentally in sodium but it is known to exist in other alkali metals [23].

Hunt [22] has incorporated this effect into a modified Hicks-Menzies model by assuming that the transition occurs at the thermodynamic critical volume and allowing no further heat transfer to the sodium after the transition. He found that this reduced the predicted efficiencies significantly.

The effect of the metal-insulator transition on efficiency was investigated in the present model by terminating single phase heat transfer when the sodium specific volume exceeded $2 \times 10^{-3} m^3/kg$. This gives a bounding calculation for the effect of the metal-insulator transition since in reality the heat transfer would not be reduced to zero and the transition may not occur until about the thermodynamic critical point. Calculations for melt/sodium mass ratios of 5 and 12 showed that including the metal-insulator transition reduced the efficiencies from 8.96% to 5.55% and 6.87% to 3.62% respectively. Thus if the transition could be shown to occur at the low end of the specific volume uncertainty range the efficiencies would be reduced considerably.

If the transition is applied at the thermodynamic critical volume, as assumed by Hunt, it does not affect many of the calculated results because the thermodynamic trajectory in the P-V plane intersects the liquid branch of the two-phase envelope. Even for a melt/sodium mass ratio of 12, which causes the thermodynamic trajectory of the sodium to intersect the vapour branch of the two phase envelope, the efficiency was only reduced from 6.87% to 6.52%.

Thus, until the exact location of the transition is known it is not possible to determine whether the effect is important or not. Even then uncertainties in the EOS for sodium need to be resolved before the effect of the metal-insulator transition can confidently be determined.

4.4 The effect of Hydrodynamic Parameters

These parameters are of two different types. Firstly, there are initial conditions, such as cover gas volume and pressure, which are preset in an experiment. Secondly, there are parameters, such as the slug length, which can be estimated from experimental data. In this section the effect of these parameters on the measured work yield and MFCI characteristics will be examined.

A computational study was carried out in order to determine the effect of sodium slug length. Table 4.3 shows the efficiency, time until vapour formation, peak pressure, slug velocity at the time of change over to an inertial load and the maximum slug velocity occuring during the expansion for various slug lengths.

L(m)	η(%)	P_{max}(MPa)	Time until vapour formation (ms)	v_{init}(m/s)	v_{max}(m/s)
0.1	7.18	83	0.22	141	340
0.2	8.32	91	0.30	124	263
0.4	8.75	92	0.46	89	191
0.8	8.96	92	0.72	61	136
1.5	8.89	92	0.71	46	98

Table 4.3: The effect of slug length

The data in the above table shows that the MFCI characteristics are influenced considerably by the slug length. This is because the slug length determines the time taken for the acoustic wave to travel to the

free surface. The peak pressure is unaffected for slug lengths greater than 0.2m because in this case it is motion of the interface between the heated and unheated sodium which limits the pressure, long before the rarefaction wave returns to relieve pressure. This would not be the case if an inertial load was used during the initial stage of the interaction, as in this case the peak pressure would increase with the slug mass [13]. The table shows that as the slug mass increases the initial and peak velocity falls. Since frictional forces are proportional to the velocity squared and the interfacial area between the slug and its surroundings the data in Table 4.3 shows that in the present calculations frictional loss is greater in longer slugs. The predicted velocity for the small slug is unrealistically large since in practice a small slug would be broken up by either surface instabilities or the cavitation effect described in section 3.2.

The predicted efficiency is not very sensitive to slug length provided the slug is sufficiently long enough to allow a large fraction of the energy in the melt to be transferred to the sodium before the return of the rarefaction wave leads to vapour production. Thus the effect of slug length depends to a large extent on the rate of energy transfer, the melt fragmentation time and the chosen friction factor. For example for a heat transfer coefficient of $10^5 W/m^2K$ the efficiency is reduced from 3.67% for a 0.8m slug to 1.41% for a 0.1m slug compared to the small change shown in Table 4.3.

All the calculations presented so far have used a friction factor of 0.008 which represents an upper bound on the value which could occur for all practical purposes. Assuming there is no friction increases the predicted efficiency of the base case calculation from 8.96% to 14.99%. At first sight this seems to be a surprisingly large difference, but reference to Table 4.3 shows that this is because of the very large calculated slug velocities (~140m/s). Repeating the calculation for a heat transfer coefficient of $10^5 W/m^2K$ shows that the difference in efficiency for a less energetic interaction (which produces slug velocities closer to those observed experimentally) is much smaller, changing the efficiency from 3.67% to 5.26%. This again demonstrates how

the choice of heat transfer parameters can effect the significance of other parameters.

The difference in efficiency between a calculation with friction and one with no friction would be reduced even further if a hydraulic diameter of 1m were used instead of 0.1m, the former value being the appropriate value for the MFTF rig at Winfrith when it is used for pool-type experiments. Thus to summarize, frictional losses are important in cases where the slug hydraulic diameter is small and the interaction causes high slug velocities. For conditions closer to those observed in pool-type experiments in the MFTF, frictional forces are small. This was demonstrated by comparing two calculations with a heat transfer coefficient of $10^5 W/m^2K$ with one including friction with a hydraulic diameter of 1m and the other with no friction. The results obtained were efficiencies of 4.99% and 5.26% respectively.

4.5 The effect of Cover Gas Parameters

A series of runs were carried out to examine the effect of the choice of cover gas volume and pressure, and MFCI scale on the predicted efficiency. This is of interest because many MFCI experiments [3,14] are carried out in a closed vessel and the work done is calculated from measurements of the cover gas compression as described in section 3.5.

For example, doubling the melt mass from 5kg to 10kg caused the efficiency to be reduced from 14.99% to 13.05% with no friction and from 8.96% to 7.59% with friction. This reduction in efficiency arises because the sodium end-state pressure is higher for the larger-scale MFCI, 1.7MPa compared to 0.8MPa, showing that the MFCI could do more work if it were allowed to expand further.

Similarly, reducing the cover gas volume by a factor of 3 reduces the measured efficiency by a factor of 2/3, when zero friction was assumed. If friction is included the picture is more complicated because the piston slows down more rapidly for a smaller cover gas volume and so less energy is dissipated by friction.

Similarly, changing only the initial cover gas pressure from 0.1 MPa to 1.5MPa causes a reduction in the measured efficiency by a factor of only 14/15. However, if the sodium is assumed to be saturated at 1.5MPa the efficiency is very different due to the different initial temperature, specific volume and sound speed of the sodium.

Thus any differences in the work done measured in the pool-type experiments are due to different physical characteristics of the MFCI, and are not an effect of the chosen cover gas conditions. Thus the present results are in complete agreement with the conclusion of an earlier study [14], which assumed that the complicated MFCI expansion could be modelled by the isentropic expansion of an ideal gas against a piston which compressed the cover gas isentropically.

5. Discussion

The results given in the previous section show that the model can be used to make predictions for a variety of different experimental parameters, and to examine many different effects. However, the results have shown that certain areas of the modelling need to be improved or extended.

Firstly a more sophisticated heat transfer model is needed in the single phase region. A model which allows for the finite thermal diffusivity of the melt is a minimum requirement. A previous analysis [11] shows that radiation heat transfer is insignificant on the millisecond timescale compared to conduction in liquid coolant. A radiation/film boiling model may be added in the two phase region if it is thought to be necessary, but preliminary calculations show that most of the energy is transferred in the single phase region.

It is also intended to add condensation heat transfer which will reduce still further the predicted efficiencies. It will be necessary to determine when condensation can occur, and to make a realistic estimate of the surface area admitting condensation. The heat loss from the sodium in the interaction zone to its surroundings may also be modelled.

The model will also be used to examine the effect of using an improved EOS for sodium should one become available, since the present EOS was derived on an ad hoc basis. In particular the assumption of constant specific heat capacities in the supercritical region, the subcooled liquid region, and the superheated gas region will be improved if better data becomes available.

6.Conclusions

A rate limited model for molten fuel coolant interactions between melt and sodium has been developed. The model initially allows for the compressibility of a sodium slug which surmounts an interaction zone as heat is rapidly transferred to the sodium in the interaction zone and its pressure rises steeply. The calculation changes to a simple incompressible model for the slug dynamics when compressible effects become unimportant, as the pressure is reduced by expansion of the sodium in the interaction zone. A rate constant is used to specify the energy transfer to the sodium and the melt surface area is assumed to increase linearly over a user specified time. In addition the model has the novel feature that a constant mass of overgas is compressed by the sodium slug, allowing the model to simulate many MFCI experiments.

Preliminary results from the model have been used to examine the role played by parameters, such as slug length, heat transfer rate and fragmentation time. The present model has also confirmed the results obtained from a greatly simplified model of the behaviour of a system in which the MFCI compresses an overgas with a piston. Results obtained from the present model have demonstrated the importance of the choice of cover gas volume in MFCI experiments, if the peak cover gas pressure is to be used to measure the work done by the MFCI. The present results also demonstrate the importance of modelling dynamical effects, since for example the chosen slug length has a considerable effect on the pressure time history and the dynamics of the system. Calculations have been carried out to examine the effect of a possible metal-insulator transition in sodium. They have demonstrated that it is essential to know under what thermodynamic conditions the transition occurs, since with the present

uncertainty in its location the effect of the transition lies somewhere between no effect and a possible 50% reduction in efficiency.

The model results show that the heat transfer simulation is the most important uncertainty in the present model. Because the present model does not include mechanistic models for heat transfer and fragmentation the predicted pressures and work yields may greatly exceed those which could occur in practice. In particular, the base case calculation uses a heat transfer coefficient in the single phase region which is an effective upper bound. It is intended to include a mechanistic model, rather than specifying a constant heat transfer coefficient as is done at present, in a future version of the model. It is also intended to model condensation heat transfer and heat loss to the surroundings by conduction. The need for an improved EOS for sodium, particularly in the supercritical region, has been noted.

Acknowledgements

The author would like to thank Mr. Ian Cook for many helpful discussions during the course of this work, and to thank Prof. John Hunt (Reading University) and Dr. John Tait for providing information and unpublished work concerning the metal-insulator transition.

References

1. Cronenberg, A.W., Recent developments in the understanding of energetic molten fuel coolant interactions. Nuclear Safety, 21 p.319-337 (1980).

2. Hicks, E.P. and Menzies, D.C., Theoretical studies of the fast reactor maximum accident ANL-7120 (1965).

3. Bird, M.J., Naylor, P and Tattersall, R.B., Experimental studies of thermal interactions between thermite generated molten fuel and sodium. Paper presented at the LMFBR topical meeting, Lyon, France, July 19-23, 1982.

4. Wright, R.W., Cho, D.H., Acoustic and inertial constraints in molten fuel coolant interactions. Trans. Am. Nucl. Soc., 13, p.658-659, 1970.

5. Fishlock, T.P., EXPEL - A computing module for molten fuel/coolant interactions in fast reactor subassemblies. AEEW-R1029 (1975).

6. Cho, D.H., Chen, W.L. and Wright, R.W., Parametric study of pressure generation and sodium slug energy from molten fuel coolant interactions ANL-8105 (1974).

7. Jakeman, D., A review of the meetings of the working group on the comparison of calculational models. Paper SNI 6/21 presented to the 3rd specialist meeting on sodium-fuel interaction in fast reactors, Tokyo, Japan, March 1976.

8. Cho, D.H., Ivins, R.O. and Wright, R.W., A rate-limited model of molten fuel/coolant interactions: Model development and preliminary calculations ANL-7919 (1972)

9. Caldarola, L., A theoretical model for the molten fuel-sodium interaction in a nuclear fast reactor. Nucl. Eng. and Design, 22 p.175-211 (1972).

10. Caldarola, L., A theoretical model with variable masses for the molten fuel-sodium thermal interaction in a nuclear fast reactor. Nucl. Eng. and Design, 34, p.181-201, (1975).

11. Fletcher, D.F., Modelling transient energy release during molten fuel coolant interactions. AEEW-R2125 (1984)

12. Cole, R.H., Underwater explosions, Dover Publications, New York, 1948.

13. Fletcher, D.F., Modelling the transient pressurization during a molten fuel coolant interaction. AEEW-M2126 (1984)

14. Fletcher, D.F., A simple model of the dynamics of the MFTF rig when used for pool experiments. AEEW-M2124 (1984).

15. Browning, P., An equation of state for sodium. AERE-R9847 (1981)

16. Alderson, M.A.H.G., An equation of state for use with sodium Part 1 - Theory and Computer Program. SRD-R50 (1975).

17. Fink, J.K., and Leibowitz, L., Thermophysical properties of sodium. ANL-CEN-RSD-79-1. (1979).

18. Zemansky, M.W., Heat and Thermodynamics, McGraw Hill, London, 1968.

19. Numerical Algorithm Group Subroutine Library, Routine DØ2YAF.

20. Franz, J.R., Metal-insulator transition in expanded alkali-metal fluids and alkali-metal rare gases. Phys. Rev. B 29 p.1565-1574 (1984).

21. Ferraz, A., March, N.H., and Flores, F., Metal-insulator transition in hydrogen and in expanded alkali metals. J. Phys. Chem. solids, 45 p.627-635 (1984).

22. Hunt, J.N., Private communication (to be published) 1985.

23. Hensel, F., The nature of the critical point phase transition in metals. Mat. Res. Soc. Proc., 22, p.3-12 (1984).

Appendix I : Parameter and Initial Conditions for the Base case calculation.

This appendix lists all the data needed in the base case calculation.

Melt

Heat capacity	C_m	= 503 J/kg K
Mass	m_m	= 5kg
Temperature	T_{mo}	= 3500K
Density	ρ_m	= 8700 kg/m^3

Sodium

Pressure	P	= 0.1 MPa
Specific volume	v_s	= 1.354×10^{-3} m^3/kg
Temperature	T_{so}	= 1156 K
Sound speed	C_o	= 2100 m/s

Specific heat at constant volume

subcooled	C_v	= 1000 J/kg K
supercritical	C_v	= 850 J/kg K

superheated $C_v = 700$ J/kg K .

Melt mass/sodium mass = 5

Heat Transfer

Single phase heat transfer coefficient $h = 10^7$ W/m^2 K

Two phase heat transfer coefficient $h = 10^3$ W/m^2 K

No metal-insulator transition

Fragmentation

Fragmentation time constant $\tau_f = 1$ ms

Final melt particle size $d_p = 250$ μm.

Hydrodynamics

Slug length $L = 0.8$m

Slug interfacial area $S = 0.1\text{m}^2$

Slug hydraulic diameter $D_H = 0.1$m

Friction factor $C_f = 0.008$

Cover gas pressure $P_{cgo} = 0.1$ MPa

Cover gas volume $V_{cgo} = 0.25\ \text{m}^3$

Isentropic exponent $\gamma_{cg} = 1.67$

Appendix II : A list of Calculations Performed

Run	Conditions	Efficiency (%)
1	Base case	8.96
2	$m_m/m_s = 2$	7.46
3	$m_m/m_s = 9$	7.94
4	$m_m/m_s = 12$	6.87
5	$h_{sp} = 10^6$ W/m^{2}K	8.17
6	$h_{sp} = 10^5$ W/m^{2}K	3.67
7	$h_{tp} = 0.0$	8.65
8	$\tau_f = 0.0$	8.35
9	$\tau_f = 5$ms	8.61
10	$\tau_f = 10$ms	8.17
11	$\tau_f = 0.0$, $h_{sp} = 10^5$ W/m^{2}K	4.74
12	$\nu_{MI} = 2 \times 10^{-3}$ m^3/kg	5.55
13	$\nu_{MI} = 2 \times 10^{-3}$ m^3/kg, $m_m/m_s = 12$	3.62
14	$\nu_{MI} = \nu_{crit}$, $m_m/m_s = 12$	6.52

15	$L = 0.1m$	7.18
16	$L = 0.2m$	8.32
17	$L = 0.4m$	8.75
18	$L = 1.5m$	8.89
19	$L = 0.1m$, $h = 10^5 W/m^2K$	1.41
20	$C_f = 0.0$	14.99
21	$h = 10^5 W/m^2 K$, $C_f = 0.0$	5.26
22	$D_H = 1.0m$, $h = 10^5 W/m^2 K$	4.99
23	$m_m = 10kg$, $C_f = 0.0$	13.05
24	$m_m = 10kg$	7.59
25	$V_{cg} = 0.085m^3$, $C_f = 0.0$	11.25
26	$V_{cg} = 0.085m^3$	9.35
27	$P_{cg} = 1.5MPa$, $C_f = 0.0$	14.13
28	(Saturated coolant) $P_{cg} = 1.5$ MPa	16.04

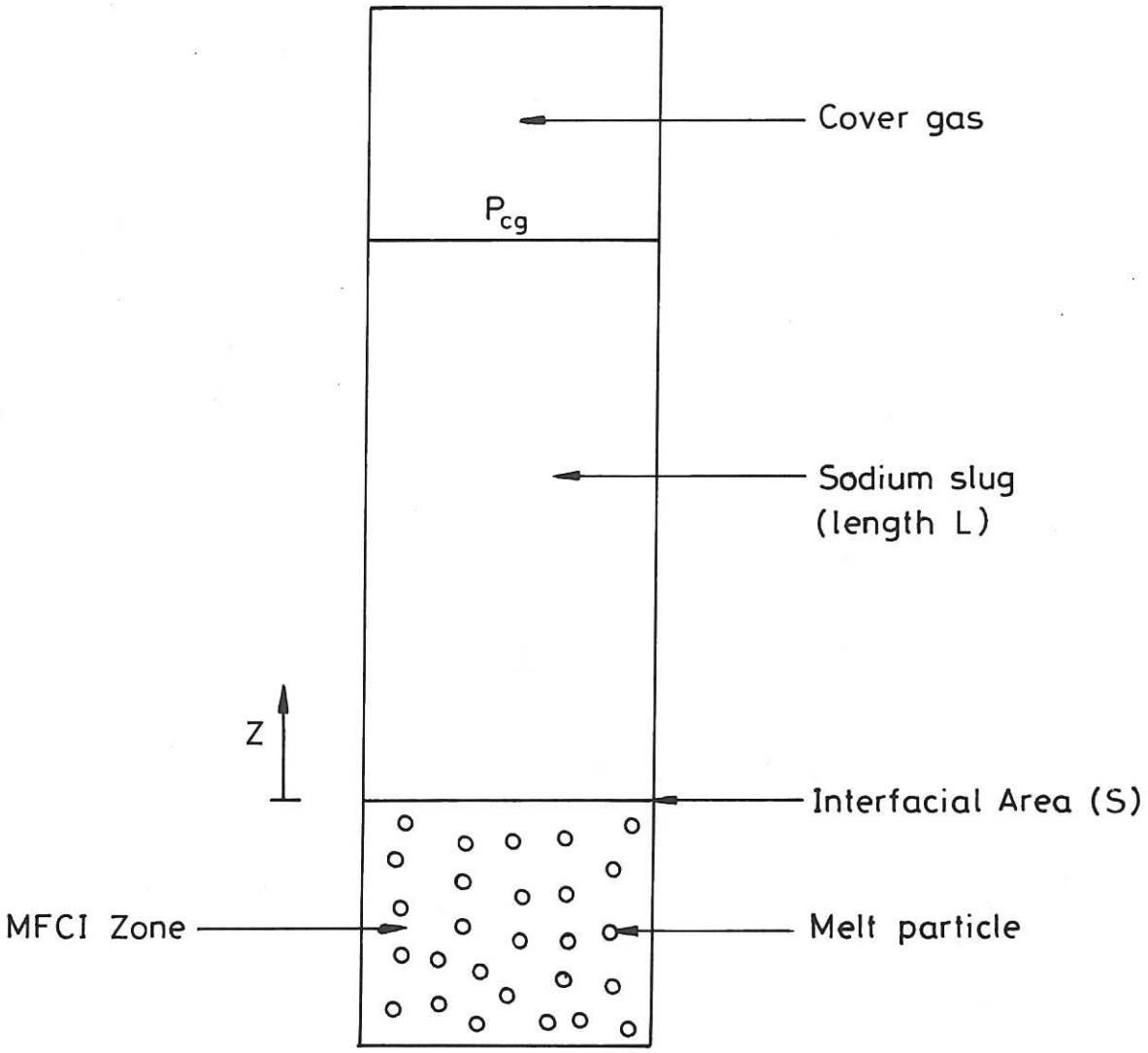

Fig. 3.1 The model geometry.

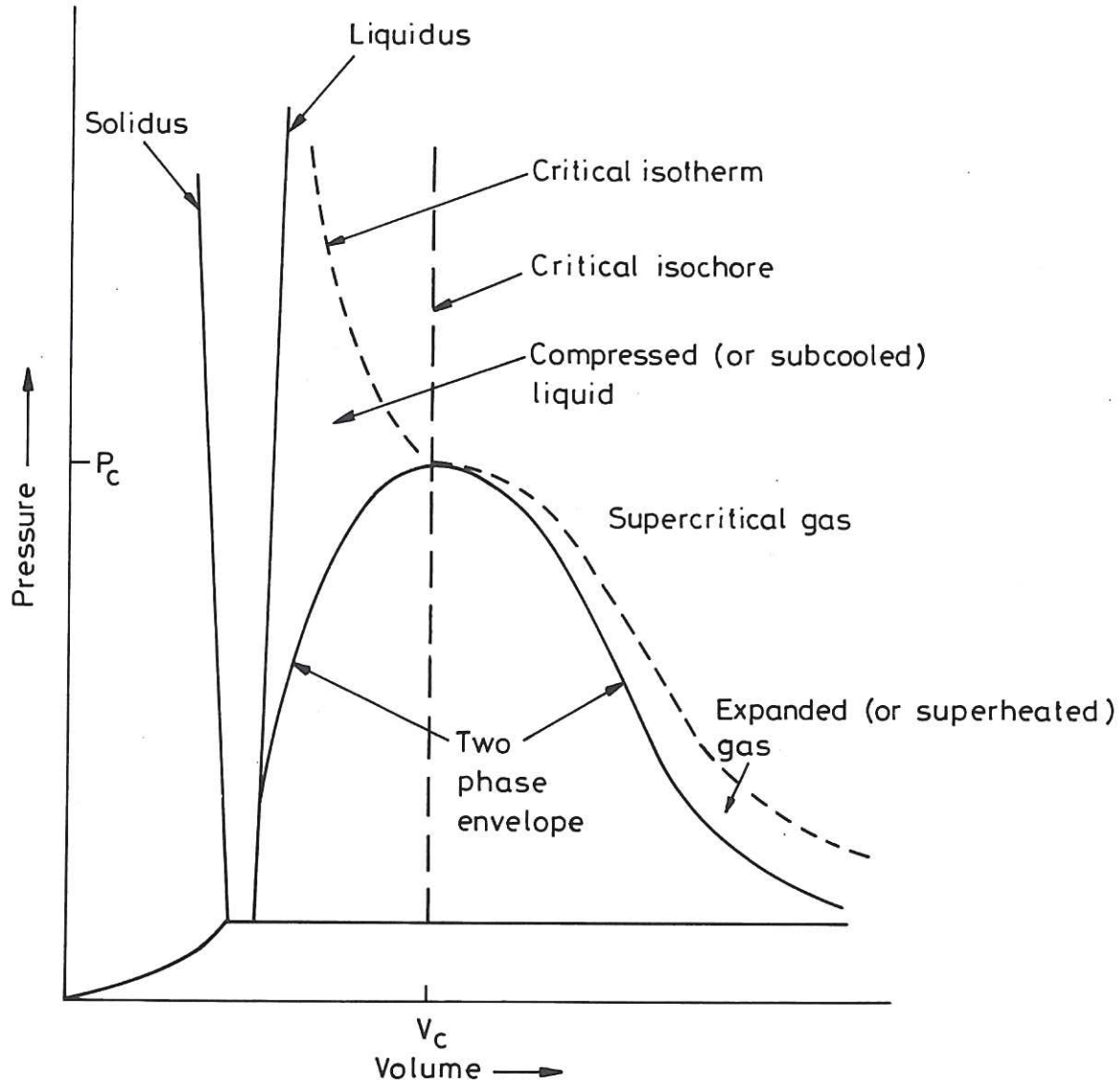

Fig. 3.2 The general P–V surface.

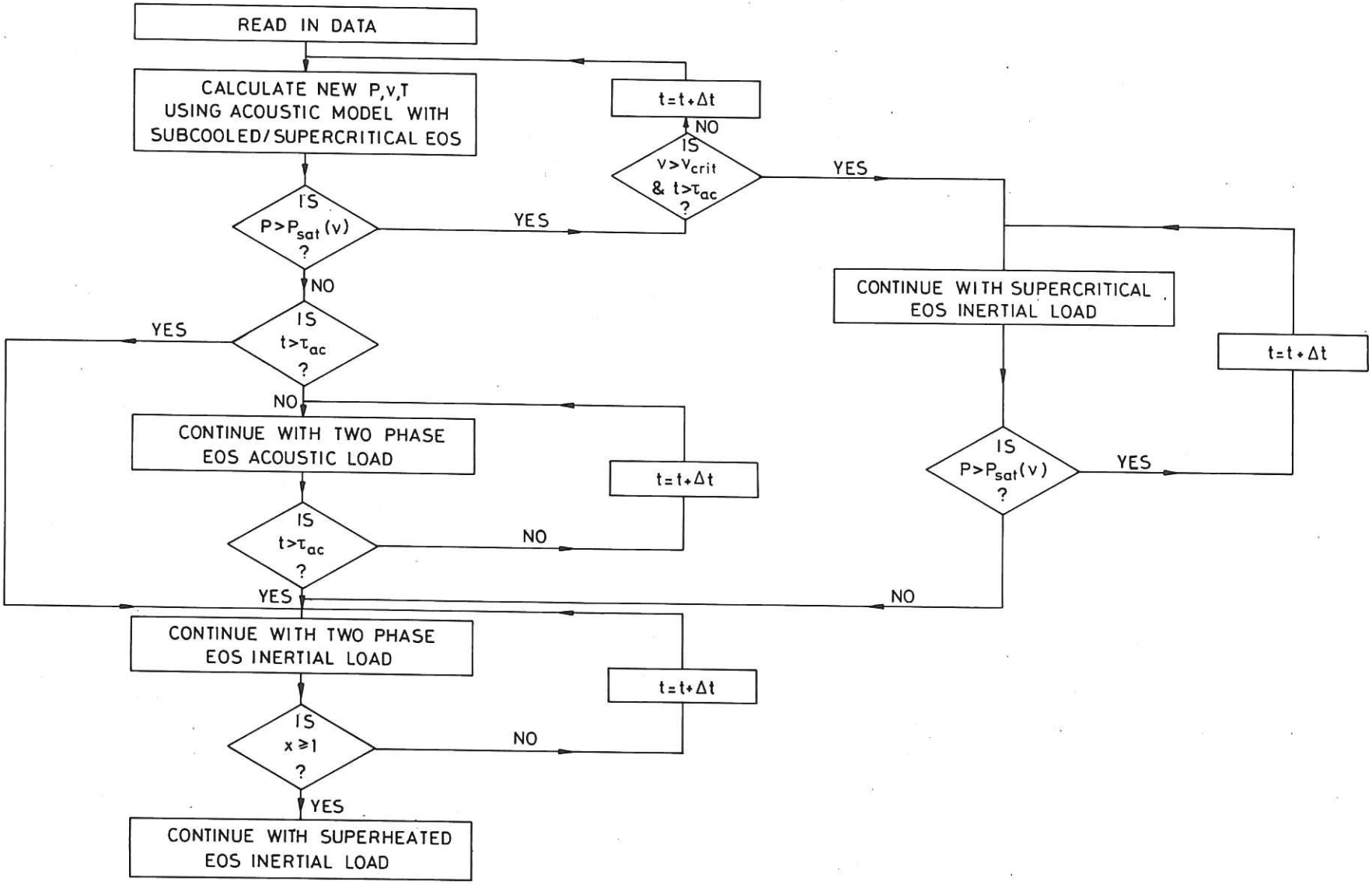

Fig. 3.3 Flow diagram for CURLIM.

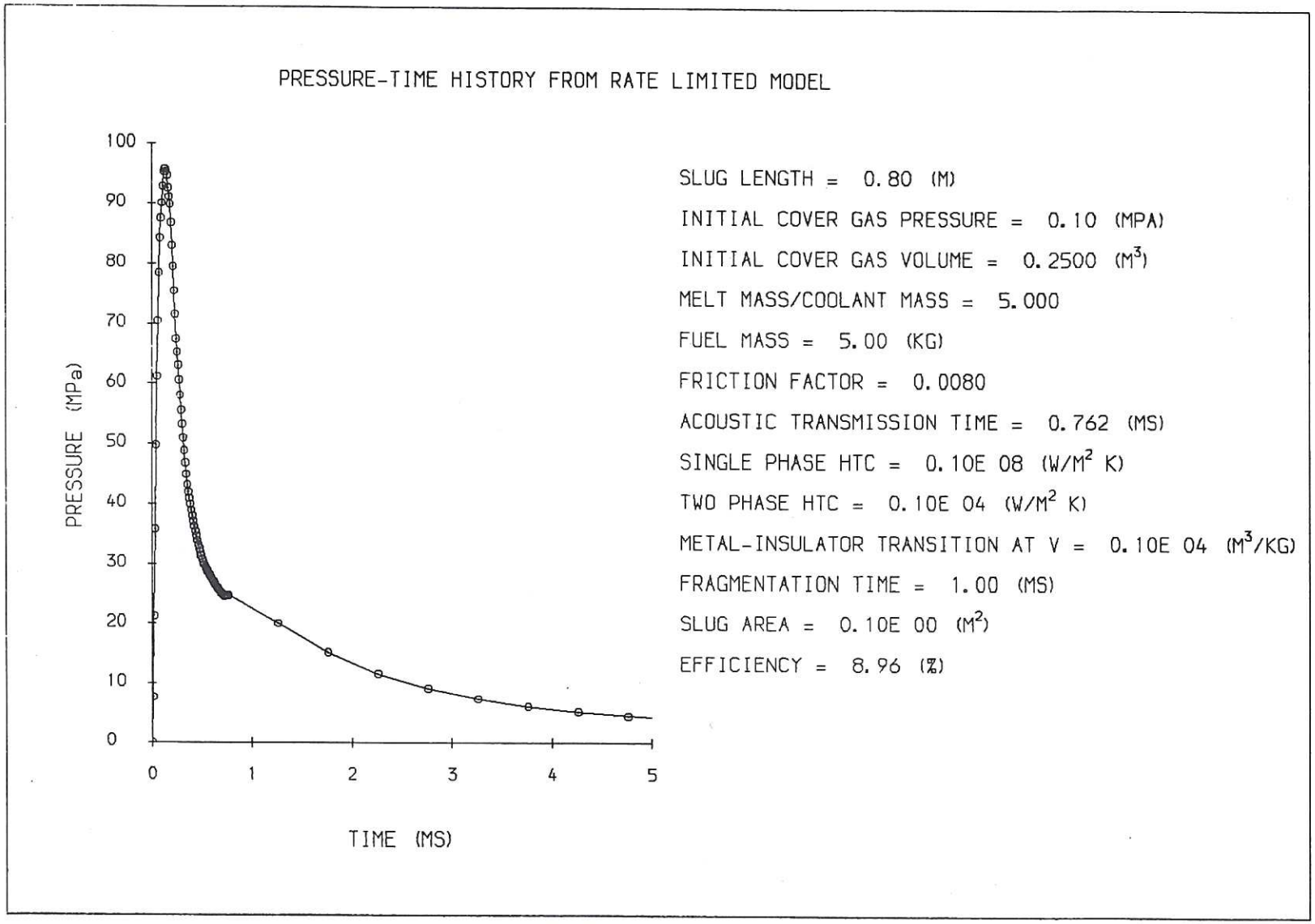

Fig. 4.1 Pressure-time plot for base case calculation.

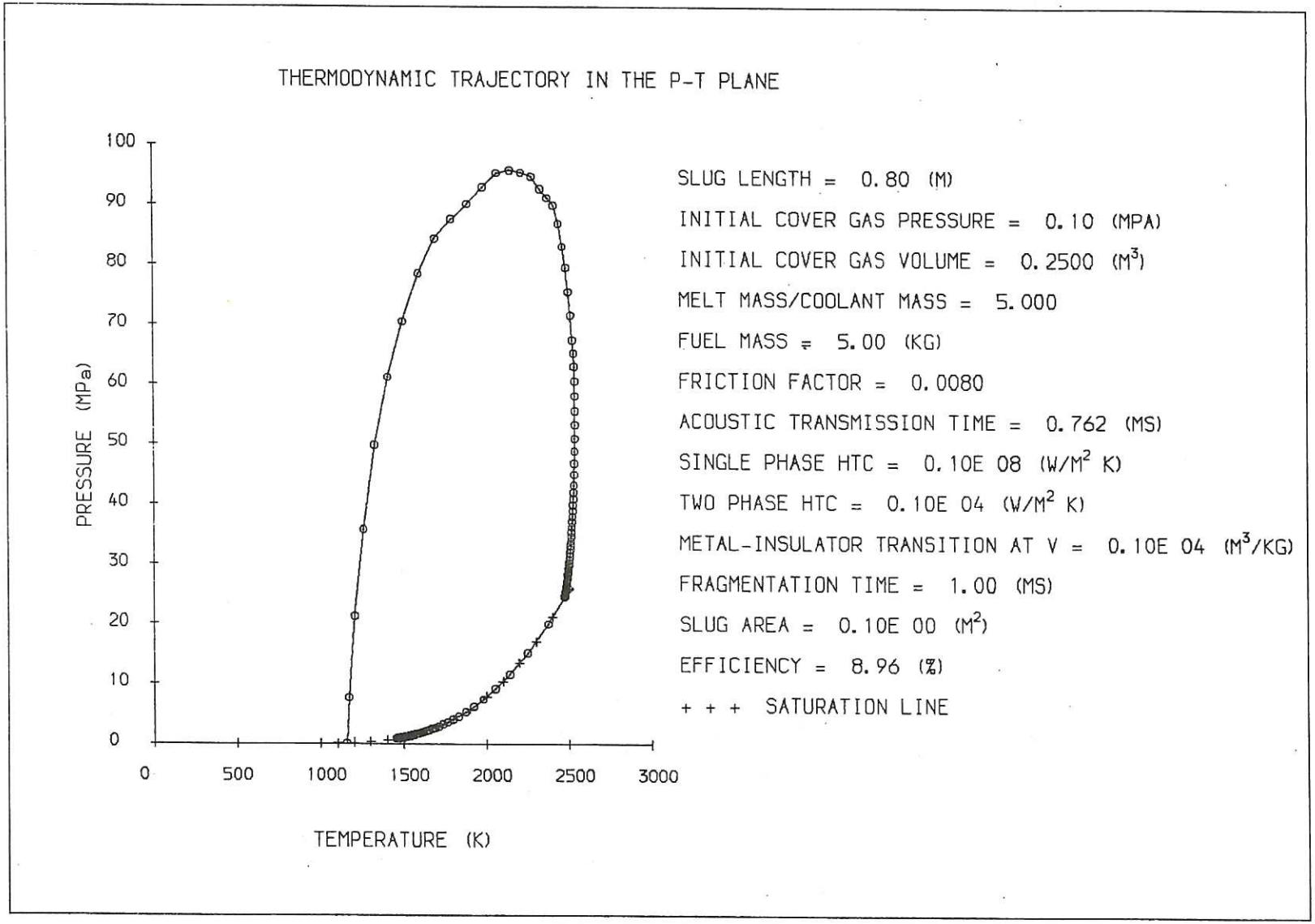

Fig. 4.2 Pressure-temperature plot for base case calculation.

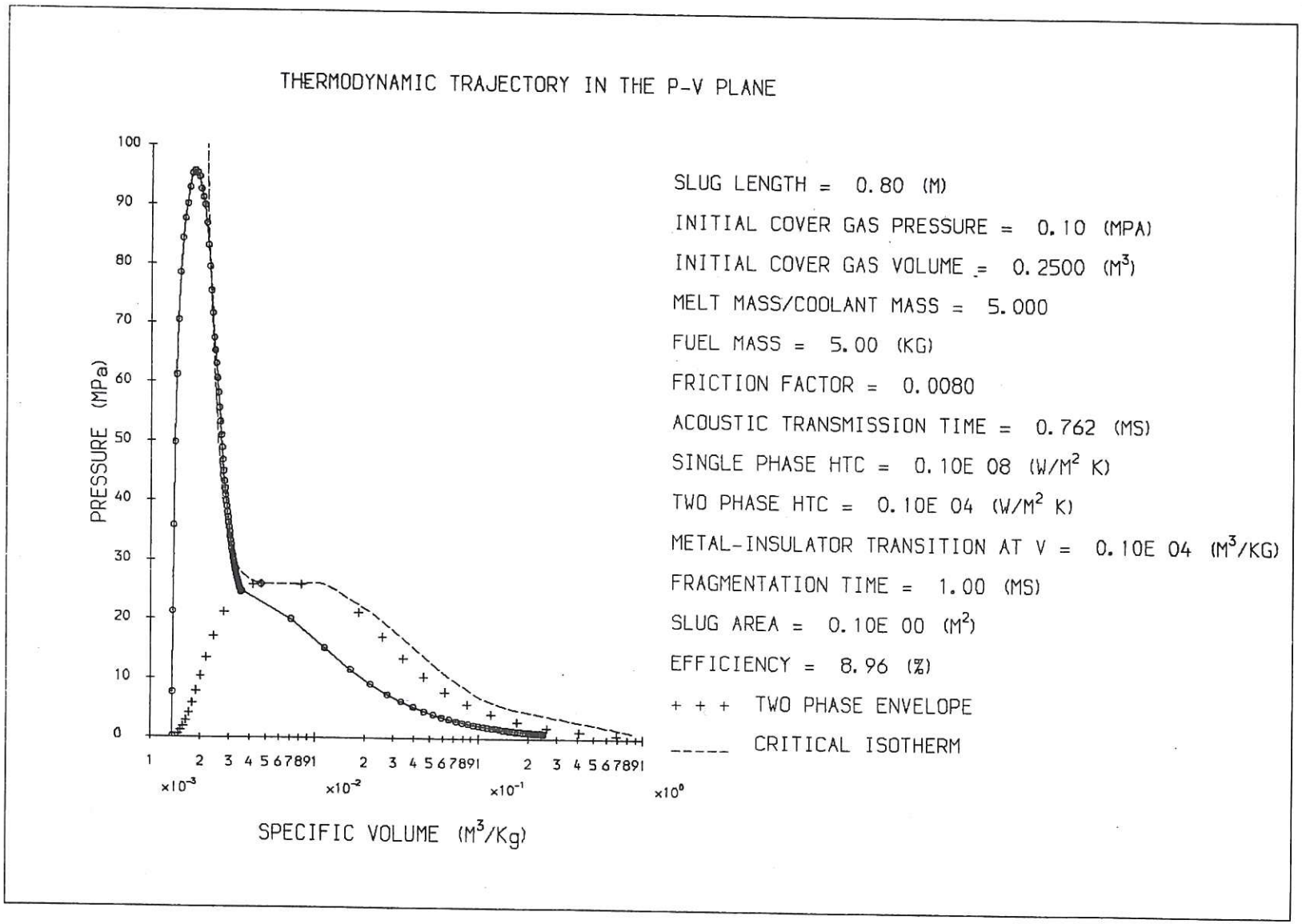

Fig. 4.3 Pressure-volume plot for base case calculation.

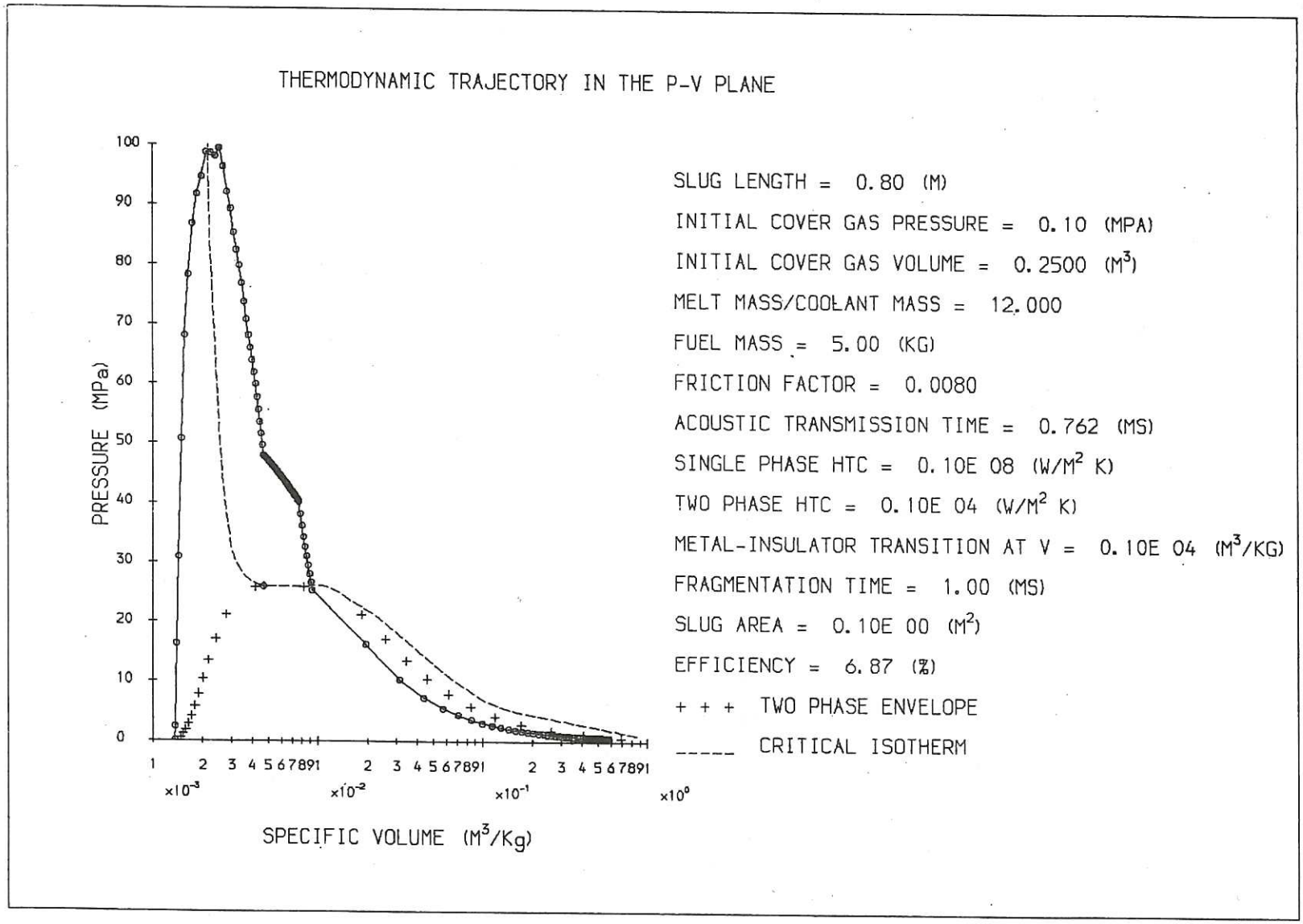

Fig. 4.4 Thermodynamic trajectory in P–V plane for a high melt/coolant mass ratio.

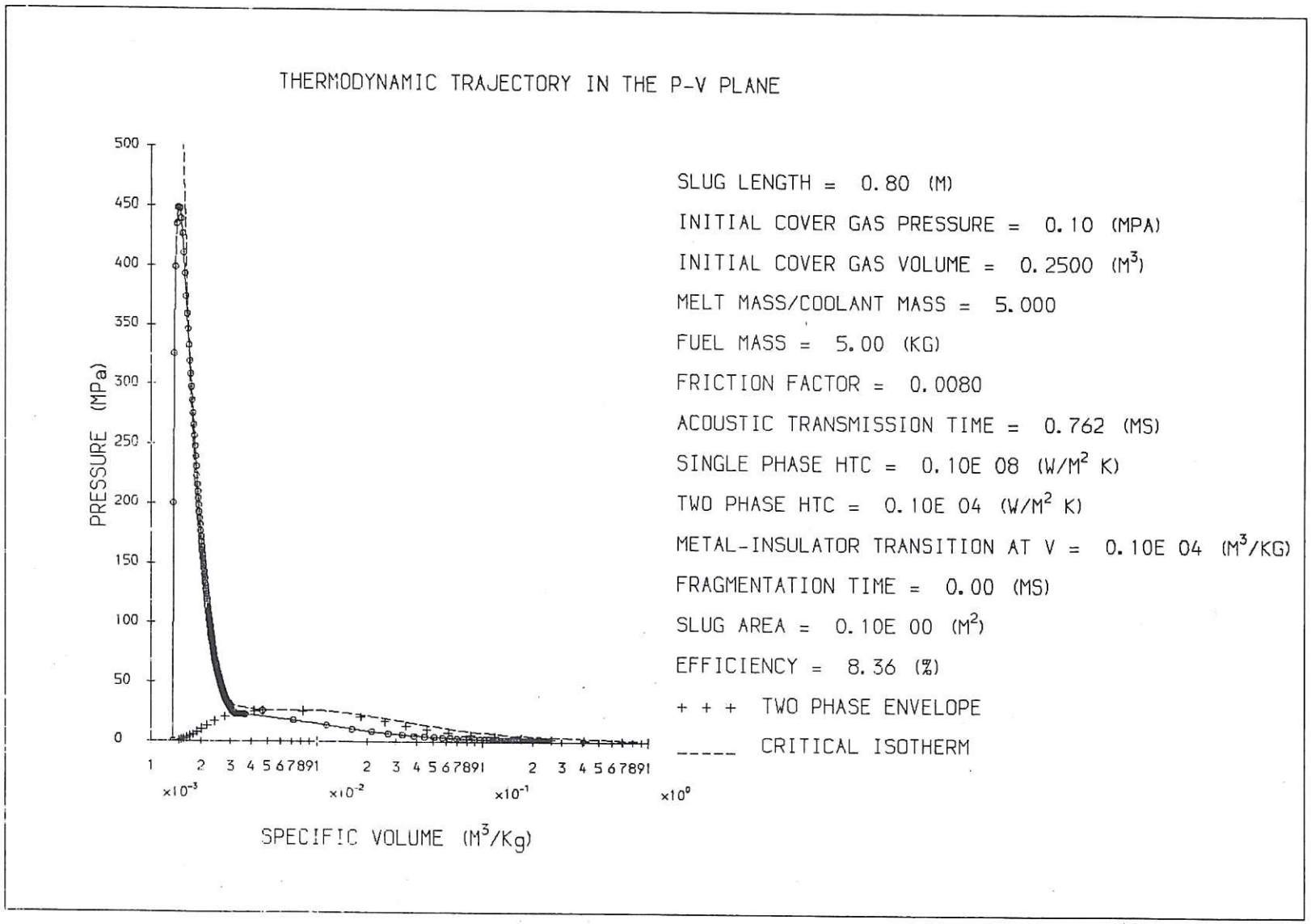

Fig. 4.5 Thermodynamic trajectory in P–V plane for instantaneous fragmentation.